ACS APPLIED MATERIALS & INTERFACES

Research Article

www.acsami.org

Multifunctional Cyanate Ester Nanocomposites Reinforced by Hexagonal Boron Nitride after Noncovalent Biomimetic Functionalization

Hongchao Wu[†] and Michael R. Kessler*[,†,‡,§]

[†]Department of Materials Science and Engineering, Iowa State University, Ames, Iowa 50011, United States

[‡]Ames Laboratory, U.S. Department of Energy, Ames, Iowa 50011, United States

[§]School of Mechanical and Materials Engineering, Washington State University, Pullman, Washington 99164, United States

ABSTRACT: Boron nitride (BN) reinforced polymer nanocomposites have attracted a growing research interest in the microelectronic industry for their uniquely thermal conductive but electrical insulating properties. To overcome the challenges in surface functionalization, in this study, hexagonal boron nitride (h-BN) nanoparticles were noncovalently modified with polydopamine in a solvent-free aqueous condition. The strong $\pi-\pi$ interaction between the hexagonal structural BN and aromatic dopamine molecules facilitated 15 wt % polydopamine encapsulating the nanoparticles. High-performance bisphenol E cyanate ester (BECy) was incorporated by homogeneously dispersed h-BN at different loadings and functionalities to investigate their effects on thermo-mechanical, dynamic-mechanical, and dielectric properties, as well as thermal conductivity. Different theoretical and empirical models were successfully applied to predict thermal and dielectric properties of h-BN/BECy nanocomposites. Overall, the prepared h-BN/BECy nanocomposites exhibited outstanding performance in dimensional stability, dynamic-mechanical properties, and thermal conductivity, together with the controllable dielectric property and preserved thermal stability for high-temperature applications.

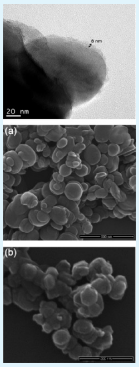

KEYWORDS: *boron nitride, polymer−matrix composites (PMCs), surface functionalization, thermo-mechanical properties, dielectric properties, thermal conductivity*

1. INTRODUCTION

Polymer composites offer excellent properties that can be tailored to specific applications and are relatively easy to process, which has made them prime candidates for a wide range of applications, from advanced microelectronic packaging to structural energy devices in aerospace engineering. To ensure appropriate service life and reliability of these devices, it is necessary to control power dissipation and heat fluxes;[1] therefore, ideal composite candidates should possess rapid heat dissipation, good electrical resistance, and low coefficients of thermal expansion (CTE).[2] Compared with most conventional thermosetting polymers, such as epoxy and polyimide, cyanate esters (CE) exhibit outstanding properties, in particular in terms of their excellent thermal stability, superior mechanical properties, and attractive low dielectric loss. Although various fillers, such as carbon nanotubes,[3−7] POSS,[8] $CaCu_3Ti_4O_{12}$,[9] and $BaTiO_3$,[10] have been investigated to improve the dielectric and mechanical properties of CE, few efforts have focused on tailoring CE's thermal conductivity.

Boron nitride (BN) is a nonoxide ceramic material with attractive physical properties, including outstanding thermal conductivity, excellent electrical insulation, desirable dielectric properties, and promising low thermal expansivity as well as superior thermal stability. For example, by utilizing its intrinsic thermal conductivity, BN was studied as an effective heat transferring medium between an electrical conductor made of CNTs/CNFs and an epoxy resin in shape memory polymer nanocomposites for Joule heating and infrared light induced shape recovery behaviors.[11,12] Compared with BN nanotubes[13−17] and BN nanosheets[18−20] that imparted outstanding properties enhancement to different polymers, h-BN nanoparticles seems to be a more appealing multifunctional fillers in epoxy,[21−24] bismaleimide resin,[25,26] polyimide,[22,27−29] and poly(vinyl alcohol)[30] for the sake of its fabrication easiness and commercial availability. Because of the chemical inertness, both covalent[16,21,31] and noncovalent[13,15,32] routes of functionalization of BN were extensively studied to enhance the dispersion and interfacial interaction between the filler and matrix prior to processing polymer nanocomposites. However, most chemical modifications of BN are very laborious and involve the use of solvents, which may cause environmental concerns. Consequently, it is essential to develop an easy and environmentally friendly route for processing and functionalization of boron nitride.

In our investigation, the functionalization of hexagonal boron nitride (h-BN) was performed using an approach inspired by the adhesive protein polydopamine, found in the anchoring mechanisms of mussels. This biomimetic polymer, which is self-polymerized from dopamine (2-(3,4-dihydroxyphenyl)-ethylamine) molecules, has been recently studied as a versatile surface coating to control the surface functionality of materials in both energy and medical devices[33,34] as well as a

Received: January 6, 2015
Accepted: March 2, 2015
Published: March 2, 2015

DOI: 10.1021/acsami.5b00147
ACS Appl. Mater. Interfaces 2015, 7, 5915−5926

modification of several nanomaterials.[35−39] The aromatic structure of polydopamine is postulated to form a strong, noncovalent bond with the hexagonal structure of BN nanotubes (BNNT) via $\pi-\pi$ and van der Waals interactions.[38] Bisphenol E cyanate ester (BECy) was selected as the polymer matrix into which both pristine and functionalized h-BN nanoparticles were incorporated for the development of advanced multifunctional polymer nanocomposites applied in microelectronic packaging and structural energy storage devices in the aerospace industry.

2. EXPERIMENTAL SECTION

2.1. Materials. Hexagonal boron nitride nanoplatelets (99%) were purchased from Nanostructured & Amorphous Materials, Inc. (Houston, TX). To avoid negative effects of residual impurities, such as metal and metal oxides, on dielectric properties,[16] the nanoplatelets were washed with prepared 10% acid solution diluted from 70% HNO_3 (reagent grade) acquired from Fisher Scientific. Dopamine hydrochloride, 2-amino-2-hydroxymethylpropane-1,3-diol (Tris), and hydrochloric acid (36% reagent) were obtained from Sigma-Aldrich (St. Louis, MO). The BECy resin used in this experiment was EX 1510 Part A and the catalyst was EX 1510 Part B, both obtained from TenCate Advanced Composites (Morgan Hill, CA).

2.2. Functionalization of h-BN Nanoparticles. Surface functionalization of h-BN nanoparticles with polydopamine followed the route reported by Thakur et al.[38] Initially, 0.726 g of Tris buffer was dissolved in a flask containing 600 mL of deionized water. Then, diluted HCl was gradually added to the solution until pH = 8.5 was reached. The solution's color turned gray as 1.2 g of dopamine hydrochloride was dissolved in the prepared 600 mL Tris-Cl aqueous solution. Subsequently, 3 g of purified h-BN nanoparticles was introduced into the solution, and the mixture was sonicated for 3 h to ensure good dispersion. The mixture was then vigorously stirred and refluxed at 60 °C for another 72 h to facilitate self-polymerization of the dopamine molecules around the h-BN nanoplatelets. After the reaction, the nanoparticles were filtered through a 0.05 μm filter membrane and washed several times with deionized water until the filtered solution became colorless. Finally, the polydopamine-treated h-BN nanoparticles were dried in a vacuum oven at 80 °C for 24 h. The color of the functionalized h-BN nanoparticles changed from white to dark-brown, indicating that the polydopamine was successfully coated onto the nanoplatelets.

2.3. Preparation of h-BN/BECy Nanocomposites. BECy nanocomposites with different loadings of h-BN nanoplatelets were processed via the following route: predetermined amounts of pristine or dopamine-treated h-BN nanoparticles were preheated at 130 °C and ground into fine powders, and then mixed with Part A of the BECy resin in a vial according to the composition in Table 1. The suspension was sonicated in a water bath for 3 h, followed by adding Part B of the BECy resin in a ratio of 3 parts catalyst per 100 parts resin. Subsequently, the slurry was prepared by alternating tip sonication with a sonic dismembrater and high-speed mixing with a planetary mixer to ensure homogenization and deaeration. Then, the slurry was gently injected into two stainless molds using a 10 mL syringe, avoiding the creation of any bubbles. The h-BN/BECy nanocomposites were first cured at 150 °C for 2 h in a rotary oven, followed by curing at 180 °C for 2 h, and postcuring at 250 °C for another 2 h.

Table 1. Calculated Amount of Components Applied in the Processing of h-BN/BECy Nanocomposites

h-BN nanoparticles (g)	BECy, Pt. A (g)	BECy, Pt. B (g)	filler (vol %)	filler (wt %)
0.699	5.723	0.177	5	10.59
1.475	5.723	0.177	10	20.00
4.685	11.45	0.354	15	28.42

2.4. Measurement and Characterization. The morphologies of pristine and dopamine-treated h-BN nanoparticles were characterized using field emission scanning electron microscopy (FE-SEM, FEI Quanta 2250) at 20.00 kV under high vacuum. Raman spectra were recorded at room temperature in the range from 800 to 2000 cm^{-1} on a Renishaw dispersive raman spectrometer with 480 nm solid-state laser as the excitation source. A small amount of nanoparticles was finely mortared and then deposited onto a glass slide followed by manually pressing to smooth the sample before measurement. The morphology of noncovalently functionalized h-BN nanoparticles and the dispersion of nanofillers in the BECy matrix were determined using a scanning and transmission electron microscopy (STEM, JEOL 2100) instrument with an accelerating voltage of 200 kV. X-ray diffraction (XRD) patterns of h-BN nanoparticles and h-BN/BECy nanocomposites were collected using a Rigaku Ultima IV powder diffractometer with Cu Kα at 40 kV/44 mA at scan steps of 0.01° from 10° to 60°. Thermo-gravimetric analysis (TGA, Q20, TA Instruments) was employed to determine the thermal degradation of dopamine-treated h-BN and the thermal stability of h-BN/BECy nanocomposites at different h-BN loadings. A platinum pan was loaded with ca. 5 mg of sample material and heated from room temperature to 800 °C at a rate of 20 °C/min in air flow. The thermal-mechanical properties of h-BN/BECy nanocomposites were studied using thermo-mechanical analysis (TMA, Q400, TA Instruments). The prepared cubic specimens (3 × 3 × 3 mm) were first heated up to 300 °C at a rate of 5 °C/min to erase their thermal history and then cooled to 30 °C at a rate of 3 °C/min. The thermal strain behavior and the CTE of the specimens were obtained from the second heating scan to 300 °C at a rate of 3 °C/min. Rectangular (15 × 5 × 1 mm) specimens were heated from 0 to 350 °C at a rate of 3 °C/min to determine the dynamic-mechanical properties of h-BN/BECy nanocomposites using a dynamic-mechanical analysis (DMA, Q800, TA Instruments) instrument in tension mode with an amplitude of 10 μm and a frequency of 1 Hz. The thermal conductivity of circular bulk nanocomposites with diameters of 30 mm and thickness of 5 mm was measured on a thermal constants analyzer (TPS 1500) from ThermTest Inc. at room temperature. The dielectric properties of the nanocomposites were characterized using a Novocontrol dielectric spectrometer from 1 Hz to 1 MHz at room temperature. Prior to characterization, both sides of the circular specimens (diameter ~ 20 mm, thickness ~ 1 mm) were sputtered with silver in an Edwards Pirani coater. To prepare the samples for dielectric breakdown strength measurements, the circular specimens were fully sputtered with silver on the bottom surface, while 20 small spots were sputtered on the top surface using a mask. The prepared specimens were placed between the probes of a dielectric rigidity instrument from CEAST/Instron, where the upper probe was precisely positioned on the sputtered spots. The breakdown voltage for each testing spot was measured as the voltage was increased by 0.5 kV/s and the current was maintained at 10 mA.

3. RESULTS AND DISCUSSION

A possible mechanism of dopamine functionalization of h-BN nanoparticles is illustrated in Scheme 1. Boron nitride nanoparticles consist of alternating boron and nitrogen atoms forming a closed hexagonal structure, which is assumed to interact with the aromatic molecules of dopamine through $\pi-\pi$ stacking forces and van der Waals forces among amino moiety.[32,38,40] Subsequently, noncovalently bonded dopamine molecules experience alkaline induced pH-oxidation and further nucleophilic reaction associated with rearrangement to form 5,6-dihydroxyindole in aqueous solution,[33,34,41,42] followed by dopamine self-polymerization on the surface of the h-BN nanoparticles.

The morphologies of pristine and dopamine-treated h-BN nanoparticles are compared in Figure 1. The purified h-BN nanoparticle showed a circular platelet shape with diameters of

DOI: 10.1021/acsami.5b00147
ACS Appl. Mater. Interfaces 2015, 7, 5915−5926

Scheme 1. Schematic Illustration of Noncovalent Functionalization of BN Nanoparticles via Polydopamine

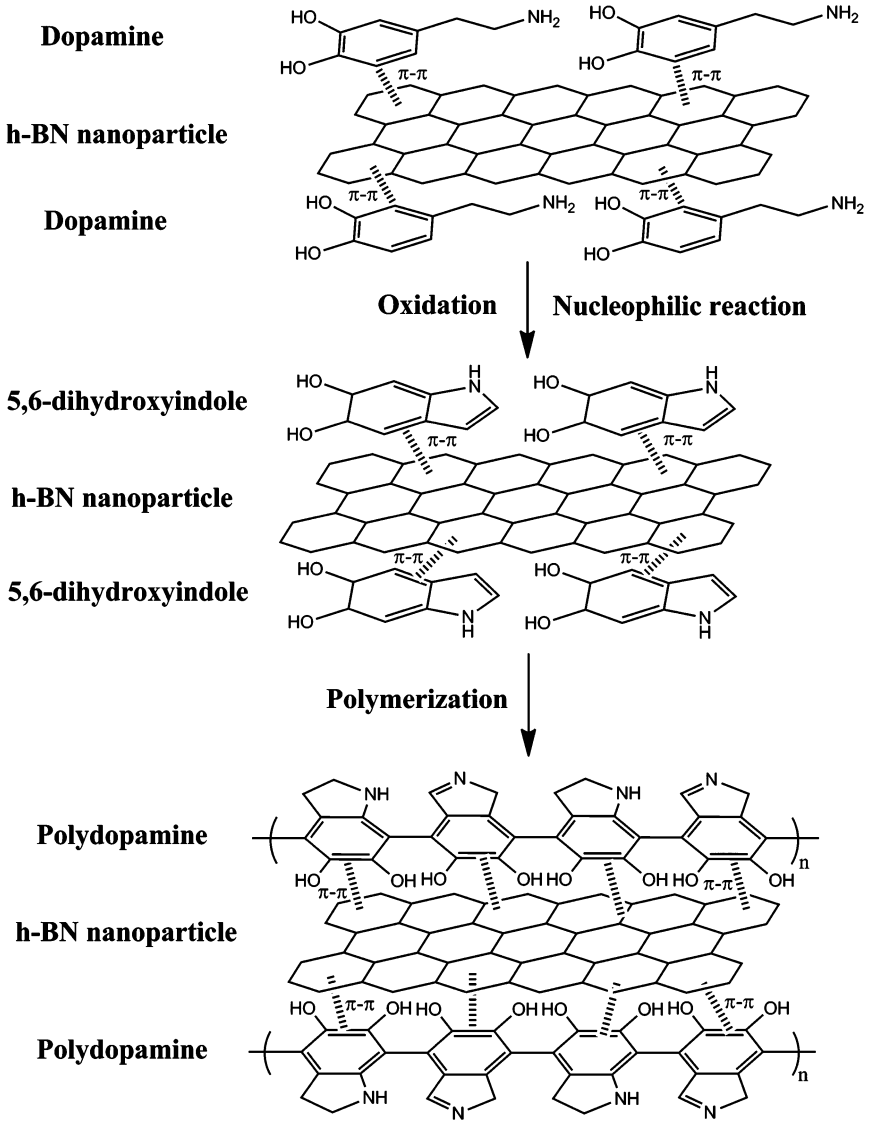

100−200 nm. The surface of the nanoparticles became rough after polydopamine functionalization compared with pristine h-BN, indicating that the polydopamine layer was noncovalently coated onto the nanoparticles.

High-resolution TEM images further confirmed the successful noncovalent functionalization of h-BN nanoplatelets by polydopamine. As shown in Figure 2, a continuous, amorphous, thin layer (ca. 8 nm) was observed on the surface of dopamine-treated h-BN nanoplatelets, indicating that the polydopamine encapsulated the nanoparticles via strong $\pi-\pi$ and van der Waals interactions.

Figure 3 compares the thermal degradation behavior of pristine and functionalzied h-BN nanoparticles. Pristine h-BN exhibited high thermal stability up to 800 °C without causing any decomposition. On the other hand, the dopamine-treated nanoparticles began to degrade at about 200 °C and then experienced major weight loss between 250 to 650 °C, which corresponded to the decomposition of polydopamine molecules attached to the surface of the h-BN nanoparticles. In addition, approximately 15% polydopamine was noncovalently attached to the h-BN nanoparticles during the surface treatment as revealed by the measured weight loss during the pyrolysis procedure.

Raman spectra in Figure 4 showed significant differences between pristine and functionalized h-BN. Pristine h-BN exhibited a sharp characteristic peak at 1366 cm^{-1}, which was attributed to the E_{2g} phonon mode.[43,44] Besides the intrinsic peak of pristine h-BN, dopamine functionalized h-BN displayd two broad peaks at 1589 and 1363 cm^{-1}, which were assigned to catechol stretching vibration and deformation in the polydopamine structure.[45,46]

Figure 5 provides a visualized comparison on the dispersion of nanosized h-BN in BECy matrix. As expected, a noticeable increasing amount of circular nanoplatelets presented when the filler loadings increased from 5 to 15 vol %. Although the surface characteristic of nanoplatelets was modified via the polydopamine treatment, the functionalization had little effect on the h-BN dispersion in polymer matrix: both pristine and dopamine-treated h-BN were homogeneously dispersed in the nanocomposites. This was attributed to the feasible processing technique applied in the experiment. It is worth noting the white scratches observed in the images, which were caused by the movement of h-BN nanoplatelets in the matrix during the

DOI: 10.1021/acsami.5b00147
ACS Appl. Mater. Interfaces 2015, 7, 5915−5926

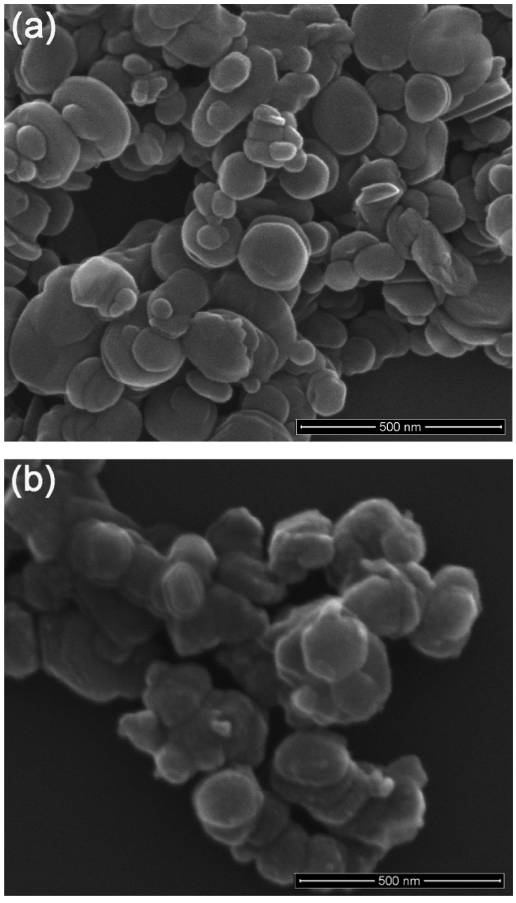

Figure 1. SEM images of h-BN nanoparticles: (a) pristine and (b) dopamine-treated.

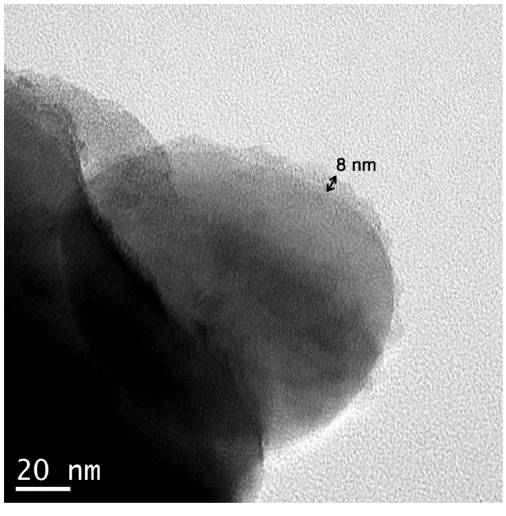

Figure 2. TEM image of dopamine-treated h-BN nanoparticles.

sectioning of ultrathin films for measurement, reflecting the high hardness of the h-BN nanoplatelets.

Figure 6 compares the XRD patterns of pristine and dopamine-treated h-BN. Pristine h-BN exhibited a well-crystallized structure, showing distinct characteristic peaks, such as the (002), (100), and (004) planes, without detection of impurity phases, indicating the high purity of the nanoparticles after the nitric acidic purification process. The dopamine-treated h-BN exhibited no major change according

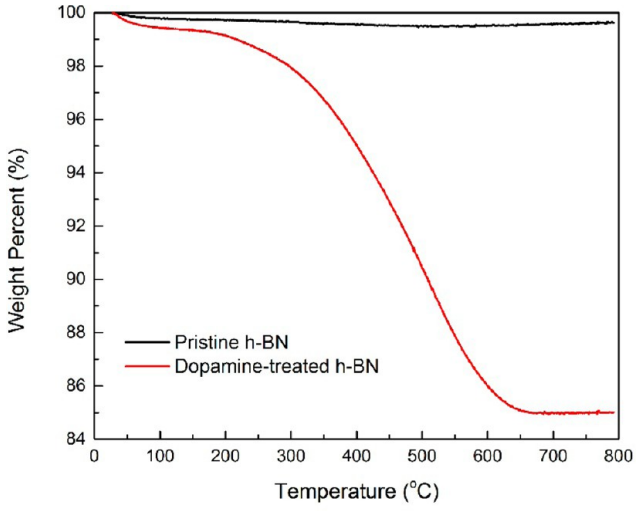

Figure 3. Thermal degradation of pristine and dopamine-treated h-BN nanoparticles.

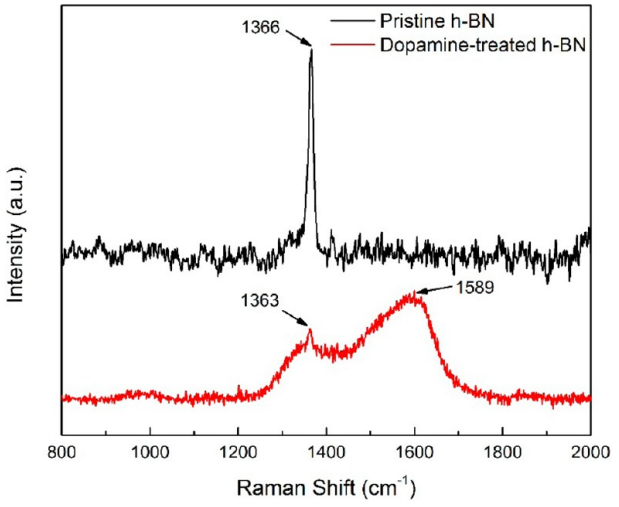

Figure 4. Raman spectra of pristine and dopamine-treated h-BN nanoparticles.

to the XRD patterns. The h-BN/BECy nanocomposites exhibited the characteristics of both the amorphous region and the intrinsic crystalline structure of hexagonal BN. Moreover, the XRD peak intensity increased as the polymer matrix incorporated higher volume fractions of nanoparticles.

TGA measurements were performed to investigate the thermal stability of h-BN/BECy nanocomposites. Both neat BECy and h-BN/BECy nanocomposites underwent thermal degradation between 450 and 700 °C, as illustrated in Figure 7, which demonstrated their prospective application in high-temperature environments. Table 2 shows that the incorporation of pristine h-BN nanoparticles at any loading level did not affect the degradation temperature, which was determined as the temperature of 5% weight loss of specimens; nonetheless, the temperature slightly decreased by 7 °C when dopamine-treated h-BN nanoplatelets were incorporated into the BECy system. The influence of the filler loading on the residual weight after the pyrolysis process at 800 °C is also summarized in Table 2. As expected, the amount of pristine h-BN nanoparticles incorporated in the samples was in a good agreement with the calculated weight percent provided in Table

DOI: 10.1021/acsami.5b00147
ACS Appl. Mater. Interfaces 2015, 7, 5915−5926

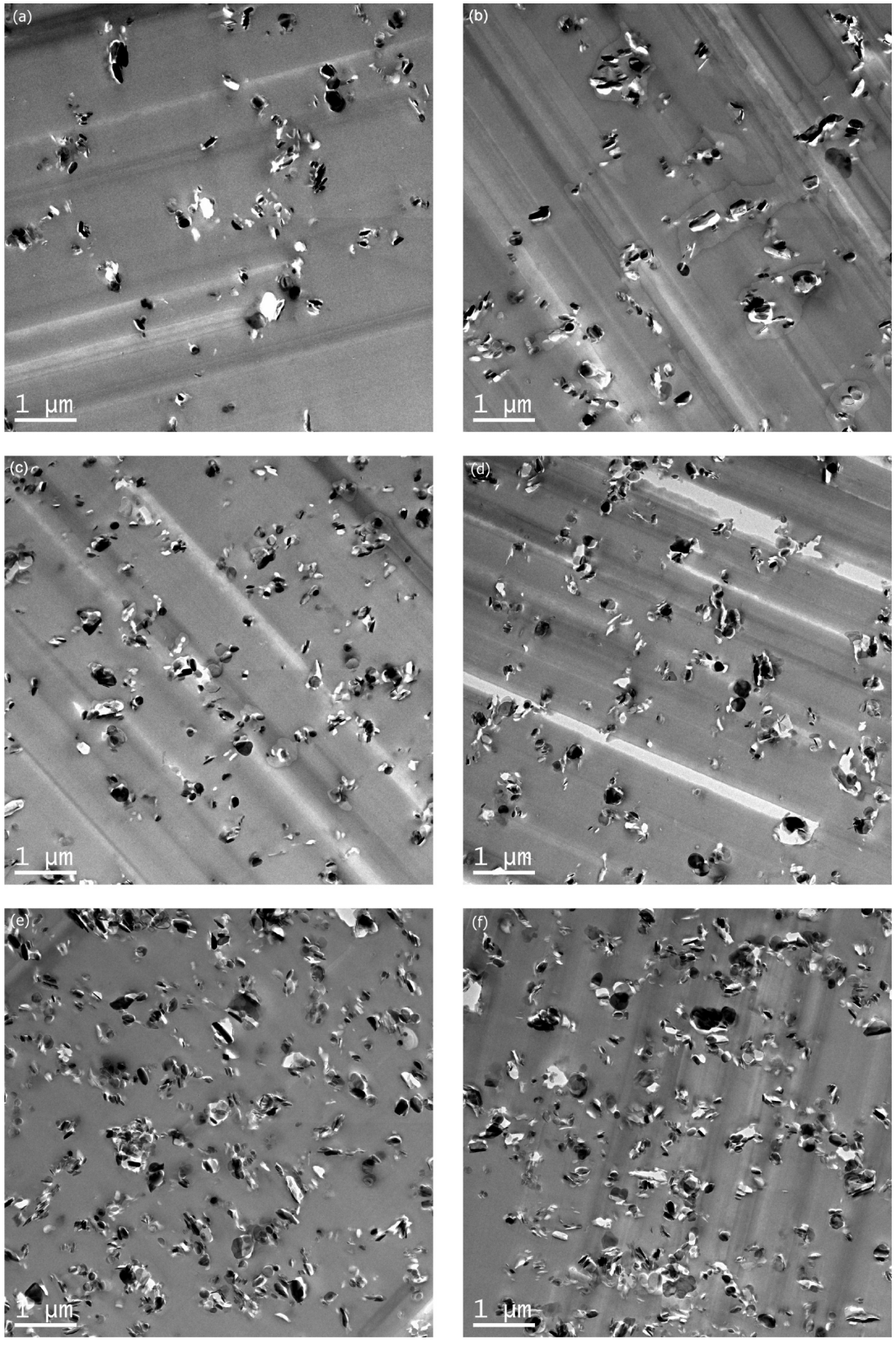

Figure 5. TEM images of h-BN/BECy nanocomposites with different functionalities and loadings: (a) 5 vol % pristine, (b) 5 vol % dopamine-treated, (c) 10 vol % pristine, (d) 10 vol % dopamine-treated, (e) 15 vol % pristine, and (f) 15 vol % dopamine-treated.

1. Regarding the polydopamine-treated h-BN, because 15 wt % polydopamine was confirmed to encapsulate the nanoparticles, it is not surprising to notice a less portion of nanoparticles left after the decomposition of nanocomposites compared with calculated values.

Figure 8 illustrates the thermal strain behavior of h-BN/BECy nanocomposites in the temperature range from 30 to 300 °C. The overall dimensional stability of BECy nanocomposites gradually improved with the incorporation of increasing volume fractions of low CTE h-BN nanoparticles (−2.7 ppm/°C),

DOI: 10.1021/acsami.5b00147
ACS Appl. Mater. Interfaces 2015, 7, 5915−5926

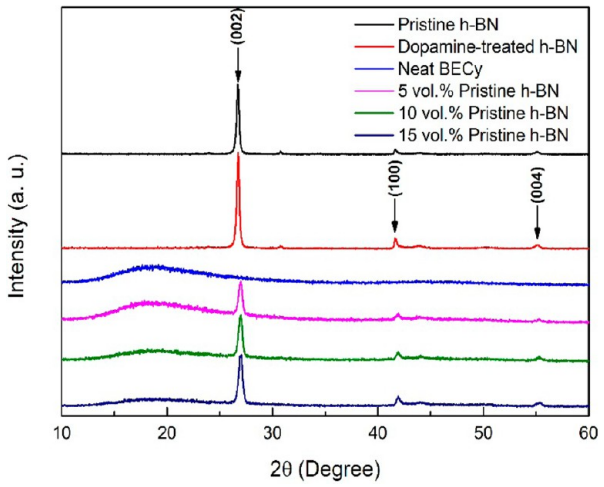

Figure 6. XRD patterns of h-BN nanoparticles, neat BECy, and h-BN/BECy nanocomposites at different filler loadings.

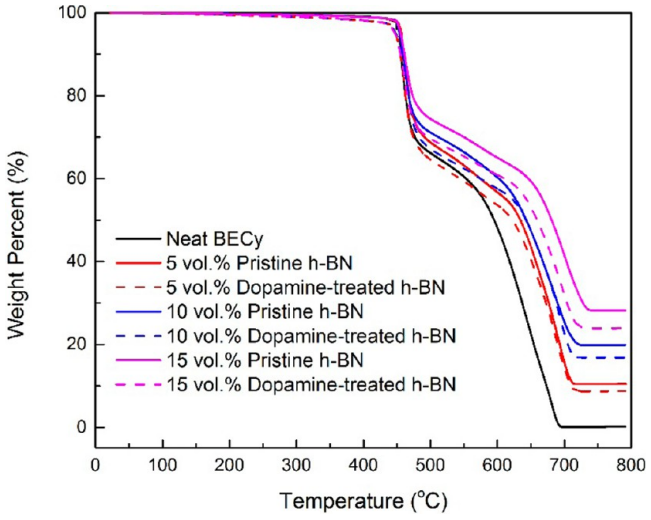

Figure 7. Comparison of thermal stability of neat BECy and h-BN/BECy nanocomposites.

indicated by the reduction in the magnitude of the slope of the thermal strain−temperature curves. Also, BECy and nanocomposites underwent a glass transition as indicated by the change in slope of the curves. Specifically, the onset of the glassy transition point was shifted to lower temperatures for the dopamine-treated h-BN/BECy nanocomposites, causing a decrease in glass transition temperature (T_g). On the other hand, the specimen reinforced by pristine h-BN nanoparticles exhibit no negative influence on T_g compared with neat BECy. The influence of nanoparticles on T_g will be discussed in more detail in the following section.

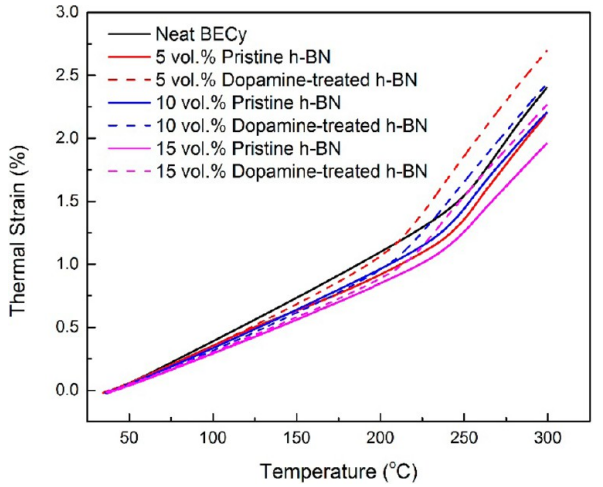

Figure 8. Thermal strain of h-BN/BECy nanocomposites.

The CTE values of h-BN/BECy nanocomposites in the glassy region were determined between 50 and 70 °C based on eq 1:

$$\alpha = \frac{L}{L_0}\frac{\mathrm{d}L}{\mathrm{d}T} \tag{1}$$

where L_0 is the initial length of the sample and L is the length at temperature T. Figure 9a compares the CTEs of nanocomposites reinforced with pristine and dopamine-treated h-BN nanoparticles at different volume fractions. Compared with neat BECy (64.9 ± 1.01 ppm/°C), the h-BN/BECy nanocomposites showed lower CTE values depending on filler loading. However, the extent of CTE reduction seemed to be independent from the functionalities of nanoplatelets at given loading levels. Figure 9b compares the experimental CTE data of pristine and h-BN reinforced nanocomposites with predictions according to different micromechanical models. Typically, three models are used to predict the CTE of polymer/filler composites. The rule of mixtures is represented by eq 2:

$$\alpha_c = \alpha_m(1 - \phi_f) + \alpha_f\phi_f \tag{2}$$

where φ_f is the volume fraction of filler, α_f is the CTE of the filler, α_m is the CTE of the matrix. Overall, the rule of mixtures overpredicted the CTEs compared with the experimental values of the nanocomposites, indicating the occurrence of interfacial interactions between the filler and the matrix in the nanocomposites. Turner's model was applied to account for the particle−matrix interactions, incorporating the bulk modulus of both filler (K_f = 450 GPa)[47] and matrix (K_m = 2.06 GPa)[48] into eq 3. However, it failed to accurately predict the CTE of these composites as it is appropriately applied only to unidirectional, fiber-reinforced composites:[49]

Table 2. Onset Thermal Degradation Temperature and Residual Weight of Neat BECy and h-BN/BECy Nanocomposites[a]

		pristine h-BN nanoparticles			dopamine-treated h-BN nanoparticles		
sample	neat BECy	5 vol %	10 vol %	15 vol %	5 vol %	10 vol %	15 vol %
temperature at 5% weight loss (°C)	455.29 ± 2.47	455.64 ± 1.02	454.16 ± 0.43	455.62 ± 0.62	448.98 ± 0.156	448.34 ± 1.53	447.50 ± 0.247
residual weight (%)	0	10.62 ± 0.017	19.88 ± 0.002	28.19 ± 0.687	8.61 ± 0.004	16.88 ± 0.006	24.11 ± 0.262

[a]The standard deviation was calculated based on four measurements.

DOI: 10.1021/acsami.5b00147
ACS Appl. Mater. Interfaces 2015, 7, 5915−5926

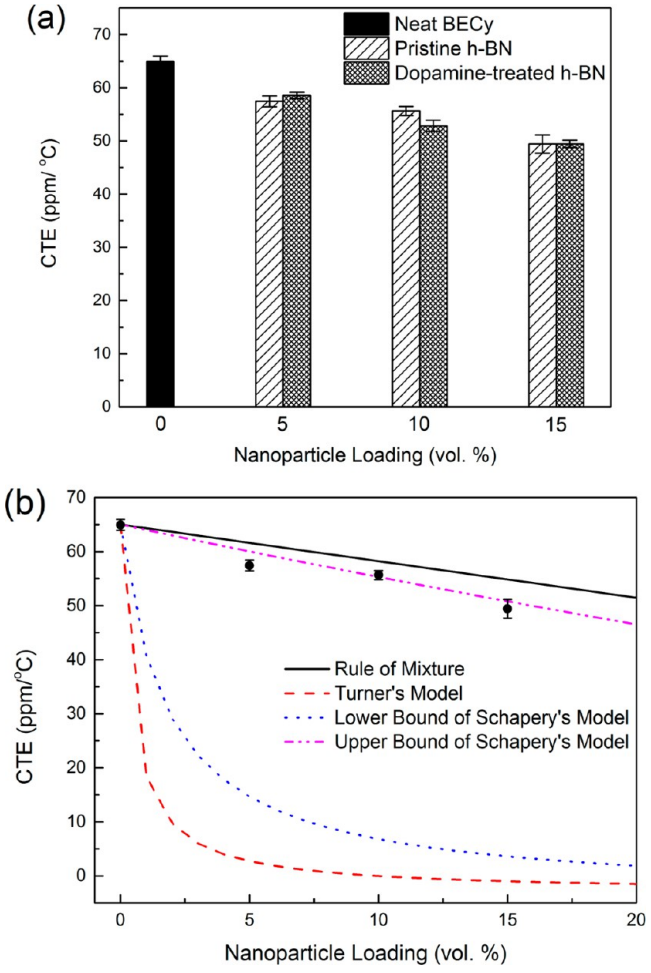

Figure 9. Thermo-mechanical properties of h-BN/BECy nanocomposites: (a) experimental CTE values, and (b) prediction models of CTE in the glassy region. The error bars represent standard deviations based on four measurements.

$$\alpha_c = \frac{(1-\varphi_f)K_m\alpha_m + \varphi_f K_f \alpha_f}{(1-\varphi_f)K_m + \varphi_f K_f} \quad (3)$$

Schapery's model includes a determination of the upper (α_c^u) and lower bound (α_c^l) values for the composites, as shown in eqs 4 and 5:

$$\alpha_c^u = \alpha_m + \frac{K_f}{K_c^l}\frac{(K_m - K_c^l)(\alpha_f - \alpha_m)}{(K_m - K_f)} \quad (4)$$

$$\alpha_c^l = \alpha_m + \frac{K_f}{K_c^u}\frac{(K_m - K_c^u)(\alpha_f - \alpha_m)}{(K_m - K_f)} \quad (5)$$

where K_c^u and K_c^l are determined using eqs 6 and 7:

$$K_c^l = K_m + \frac{\phi_f}{\frac{1}{K_f - K_m} + \frac{3(1-\phi_f)}{(3K_m + 4G_m)}} \quad (6)$$

$$K_c^u = K_f + \frac{1-\phi_f}{\frac{1}{K_m - K_f} + \frac{3\phi_f}{(3K_f + 4G_f)}} \quad (7)$$

where G_m and G_f are the shear moduli of the matrix (0.78 GPa)[48] and the filler (112 GPa),[47] respectively. The upper bound of Schapery's model provided a very close approximation of the CTE values for h-BN/BECy nanocomposites. In addition, Schapery's upper limit also provided good predictions of the CTE behavior for the BECy matrix reinforced by other nanofillers.[48,49]

The dynamic-mechanical properties of BECy nanocomposites reinforced by h-BN nanoparticles are displayed in Figure 10. Figure 10a shows that the reinforcing effect of the

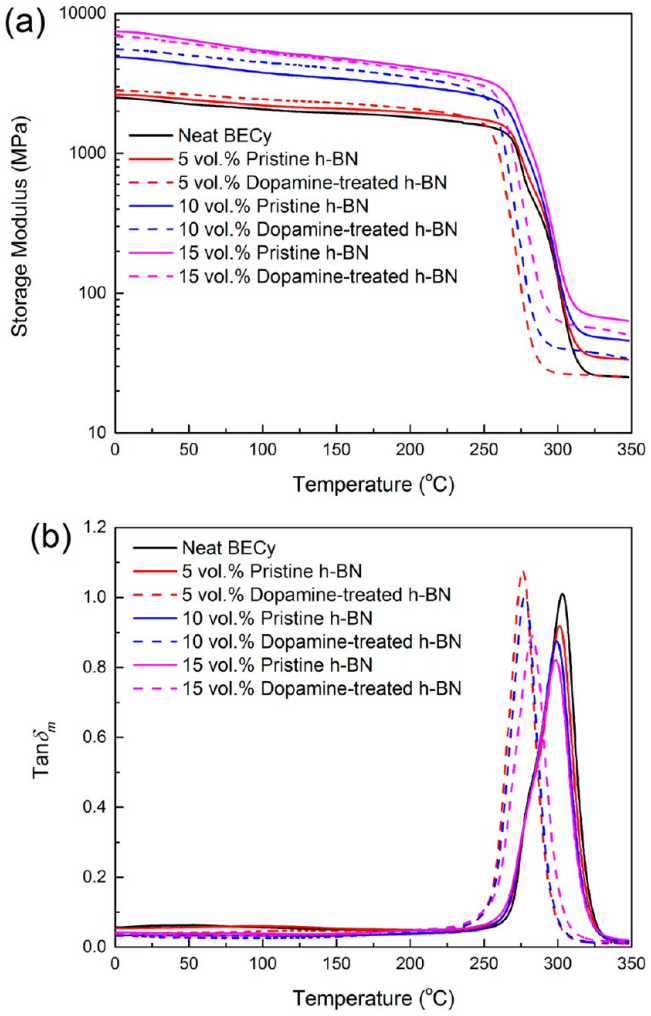

Figure 10. Dynamic mechanical properties of h-BN/BECy nanocomposites: (a) storage modulus, and (b) tan δ_m.

nanoparticles as recognized by a gradual increase in dynamic storage modulus (E') in both glassy and rubbery regions with increasing loading levels of h-BN particles. In Figure 10b, a decreasing trend of tan δ_m peak's magnitude with increasing filler loading was detected regardless of the nanoparticles' functionality. Such phenomena could be a consequence of alleviating the damping effect by enhancing the elastic response of stress transferring within BECy as elastic fillers incorporated into the viscoelastic matrix.[50] Furthermore, T_g is often taken at the tan δ_m peak temperature; therefore, dopamine-treated h-BN reinforced nanocomposites exhibited a slightly T_g suppression by 20−25 °C compared with neat BECy (~300 °C). In contrast, pristine h-BN had almost no negative effect on T_g, as illustrated from tan δ_m peak position in Figure 10b. According to several previous studies, the reduction in T_g was also found in BECy nanocomposites reinforced by various nanofillers, such as alumina,[51] ZrW_2O_8,[48] and Fe_3O_4 coated SiO_2,[52] which might

DOI: 10.1021/acsami.5b00147
ACS Appl. Mater. Interfaces 2015, 7, 5915−5926

be interpreted by the weak interfacial interaction between fillers and matrix based on an "interphase creation" theory proposed by K. Putz et al.[53] In this study, pristine nanoparticles had nearly no detrimental effect on the T_g of BECy nanocomposites at any given volume fractions, which was attributed to the formation of covalent bonding between the primary amine moiety ($-NH_2$) terminated on the nanoparticles' surface[54] and the $-OCN$ group of the cyanate ester.[9,10] After the dopamine functionalization, however, a number of flexible hydroxyl ($-OH$) and secondary ($R-NH-R$)/aromatic amine ($=N-R$) groups formed on the polydopamine shell increased the molecular chains segmental mobility of BECy, and thus led to a reduction in T_g of functionalized h-BN nanocomposites.[55]

Figure 11a depicts the effect of functionalities and volume fractions of h-BN on E' of BECy at 25 °C. As expected, E'

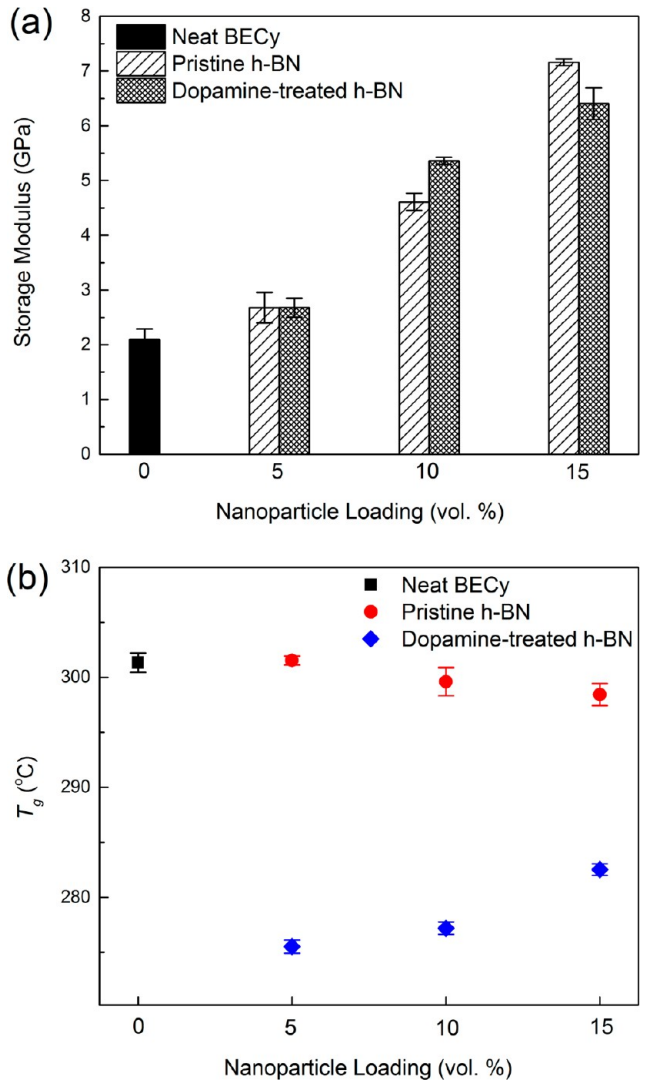

Figure 11. Comparison of (a) storage modulus at 25 °C, and (b) glass transition temperature of h-BN/BECy nanocomposites. The error bars represent standard deviations based on four measurements.

increased with higher volume fractions of nanofillers contained in the polymer matrix. The different functionalities of h-BN had little influence on E' at equivalent loading levels. For example, although nanocomposites reinforced by both types of h-BN at 5 vol % exhibited the same increase in E' (27%), at higher loading levels (10 vol %), the dopamine-treated nanoparticles facilitated a higher increase in E' than pristine h-BN at (156% vs 120%). The storage modulus reached its highest value of 7.16 GPa for nanocomposites reinforced with 15 vol % pristine h-BN nanoparticles, which doubled the value of neat BECy. As depicted in Figure 11b and discussed earlier, pristine h-BN/BECy nanocomposites present overall higher T_g than the specimen containing same volume faction of the dopamine-treated nanoparticles.

Figure 12a illustrates the thermal conductivity of h-BN/BECy nanocomposites. The high thermal conductivity (600

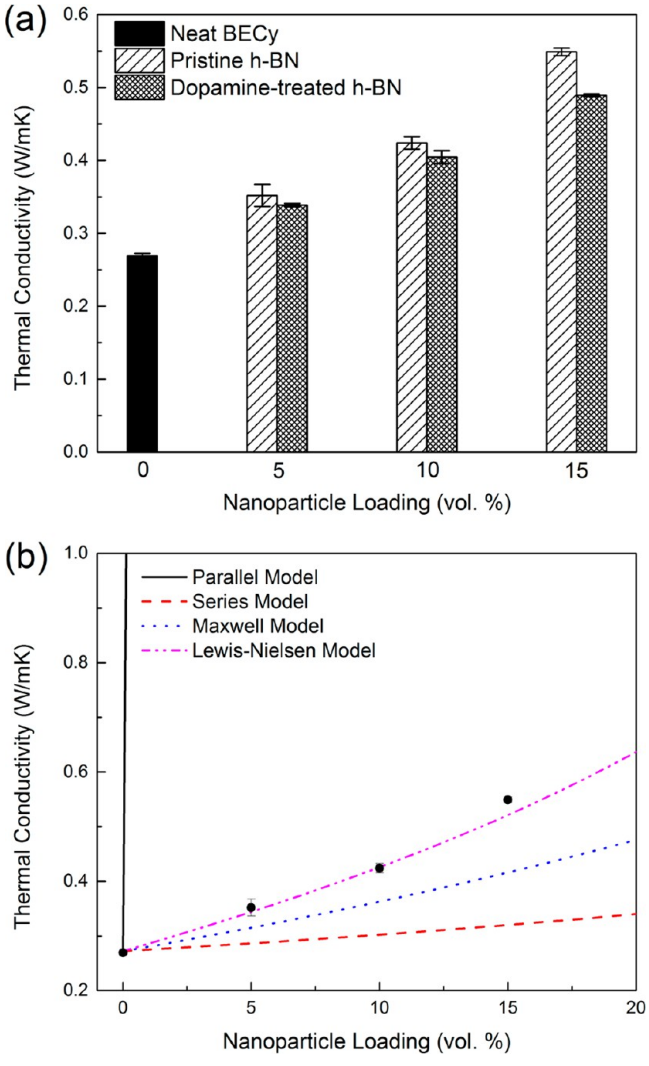

Figure 12. Thermal conductivity of h-BN/BECy nanocomposites: (a) experimental values, and (b) prediction models of thermal conductivity. The error bars represent standard deviations based on three measurements.

W/(m·K)) of the incorporated h-BN nanoparticles facilitated an obvious increase in thermal conductivity compared to the neat BECy. The samples containing 15 vol % pristine h-BN exhibited the highest thermal conductivity, which was twice that of neat polymer (0.27 vs 0.55 W/(m·K)). It is also worth mentioning that the samples containing pristine h-BN exhibited overall higher thermal conductivity than those containing dopamine-treated nanofillers. This was attributed to a less thermally conductive polydopamine amorphous thin layer, which was found to encapsulate on the surface of functionalized

DOI: 10.1021/acsami.5b00147
ACS Appl. Mater. Interfaces 2015, 7, 5915−5926

h-BN, inhibited the effective thermal transferring between h-BN and polymer matrix.

Several theoretical and empirical models have been developed and applied to predict the thermal conductivity of polymer nanocomposites. In this study, some typical models were used to investigate pristine h-BN/BECy nanocomposites systems. Initially, simple parallel and series models were applied (see eqs 8 and 9):[56]

$$k_c = \phi_f k_f + \phi_m k_m \tag{8}$$

$$k_c = \frac{k_m k_f}{\phi_m k_f + \phi_f k_m} \tag{9}$$

where φ_f is the volume fraction of the filler, φ_m is the volume fraction of the matrix, and k_c, k_f, and k_m are the thermal conductivity of the composite, filler and matrix, respectively. Figure 12b shows that parallel and series models generally provide upper and lower bounds for the thermal conductivity of composites. The Maxwell model was also applied (see eq 10). However, the Maxwell model underestimated the experimental data, which may have been caused by the assumption that the reinforcing filler was of spherical shape.[57]

$$k_c = k_m \frac{k_f + 2k_m + 2\phi_f(k_f - k_m)}{k_f + 2k_m - \phi_f(k_f - k_m)} \tag{10}$$

Taking account of the shape, aspect ratio, and packing factor of the nanoparticles, the Lewis–Nielsen model was modified and derived from the Halpin–Tsai equation given in eq 11:[58]

$$k_c = k_m \frac{1 + AB\varphi}{1 - B\psi\varphi} \tag{11}$$

$$\text{where } B = \frac{\frac{k_f}{k_m} - 1}{\frac{k_f}{k_m} + A}, \quad \psi = 1 + \left(\frac{1 - \phi_m}{\phi_m^2}\right)\varphi$$

The shape parameter A and the packing factor ϕ were chosen as 3.99 and 0.52, respectively, for platelet-sized nanoparticles. Compared to the experimental data, the Lewis–Nielsen model offered an excellent prediction of the thermal conductivity of h-BN/BECy nanocomposites. Previous studies[57,59,60] also showed the promising thermal conductivity prediction for other composite systems.

The effects of nanoparticle functionality and volume fraction on dielectric properties of h-BN/BECy nanocomposites were examined. Figure 13a,b shows that 15 vol % pristine h-BN increased the permittivity (ε') of BECy nanocomposites by only approximately 0.2 without negative influence on the dissipation factor (tan δ_e) over a wide frequency range, which was attributed to the intrinsic dielectric properties of BN. However, dopamine-treated h-BN had a significant effect on the dielectric properties of h-BN/BECy nanocomposites; they exhibited an overall higher ε' and tan δ_e than the specimens containing pristine nanoplatelets at the same volume fraction, in particular in the lower frequency range between 1 and 10 Hz. This behavior was originated from an increase in frequency-dependent orientation polarization induced by the strong dipole–dipole moment among a sufficient number of amino moieties and catechol groups formed in the conjugated bridge structure of the polydopamine coating.[61] In addition, a substantial increase in tan δ_e at low frequencies elicited the

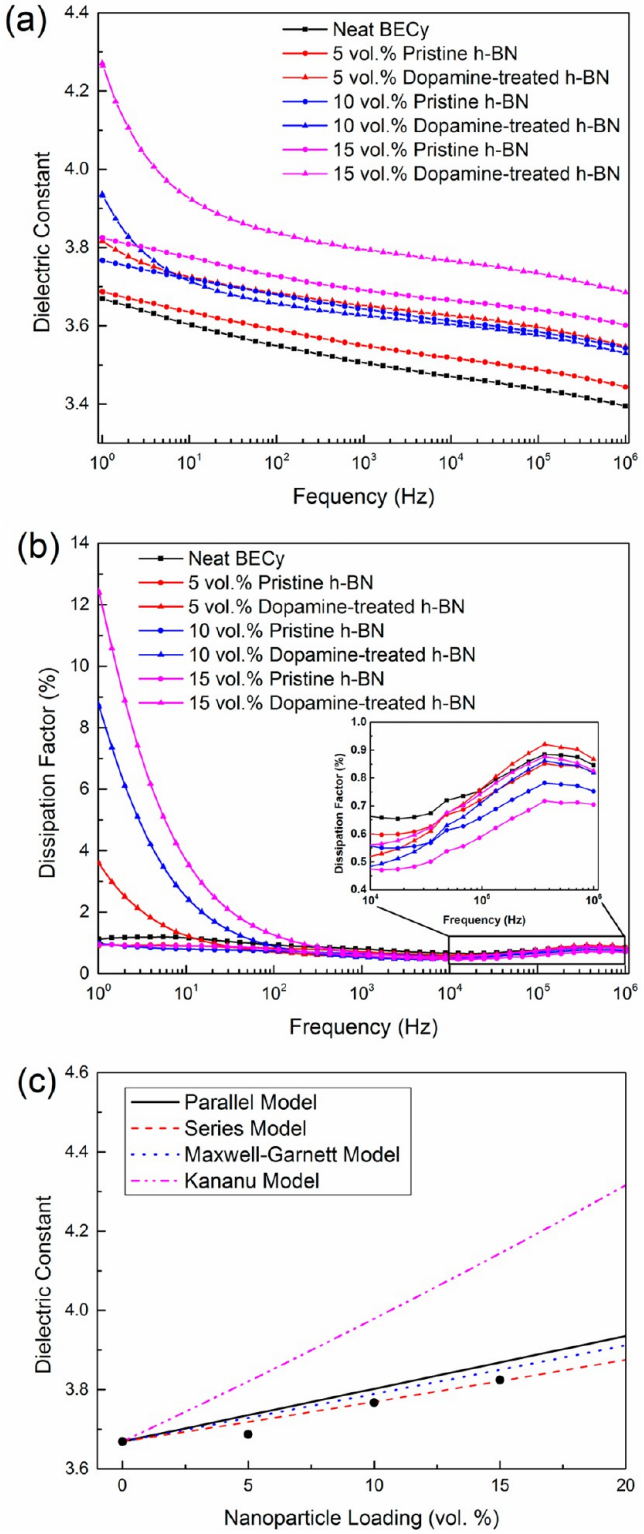

Figure 13. Dielectric properties of h-BN/BECy nanocomposites: (a) experimental dielectric constant, (b) prediction models of dielectric constant at 1 Hz, and (c) dissipation factor.

presence of space charge polarization or ionic conduction dielectric loss within nanocomposites.[55]

The dielectric constants of the investigated composite materials were predicted using both theoretical and empirical models. The two common models employed were the parallel (eq 12) and the series model (eq 13):

DOI: 10.1021/acsami.5b00147
ACS Appl. Mater. Interfaces 2015, 7, 5915–5926

$$\varepsilon_c = \phi_f \varepsilon_f + \phi_m \varepsilon_m \quad (12)$$

$$\varepsilon_c = \frac{\varepsilon_m \varepsilon_f}{\phi_m \varepsilon_f + \phi_f \varepsilon_m} \quad (13)$$

where ε_c, ε_f, and ε_c are the dielectric constants of the composite, filler, and matrix, respectively. The Kananu and the Maxwell–Garnett model are given in eqs 14 and 15 for comparison. Among them, the obtained experimental permittivity of h-BN/BECy nanocomposites at 1 Hz followed series model well.

$$\varepsilon_c = \varepsilon_m + \frac{2\phi_f \varepsilon_f \varepsilon_m}{2\varepsilon_m + \phi_m \varepsilon_f} \quad (14)$$

$$\varepsilon_c = \varepsilon_m \left[1 + \frac{3\phi_f \times \frac{\varepsilon_f - \varepsilon_m}{\varepsilon_f + 2\varepsilon_m}}{1 - \phi_f \times \frac{\varepsilon_f - \varepsilon_m}{\varepsilon_f + 2\varepsilon_m}} \right] \quad (15)$$

The dielectric breakdown strength of a material is an important property for microelectronic packaging applications. Figure 14 compares the breakdown strength of h-BN/BECy nanocomposites. It can be seen that reinforced h-BN nanoplatelets slightly improved the breakdown strength of the polymer matrix (16.94 ± 1.48 MV/m) with increasing volume fraction of nanoparticles, which was due to the higher intrinsic breakdown strength of the h-BN (35 MV/m) and homogeneous dispersion of nanoparticles on polymer matrix. The functionality of nanofillers had no significant effect on the breakdown strength of the nanocomposites.

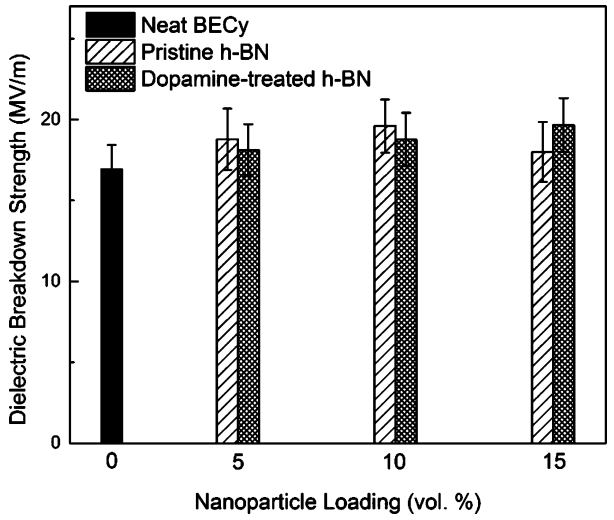

Figure 14. Comparison of dielectric breakdown voltage of h-BN/BECy nanocomposites. The error bars represent standard deviations based on 20 measurements.

4. CONCLUSION

In this work, a novel biomimetic functionalization approach was used to enhance the chemical reactivity of h-BN nanoparticles in an aqueous solution. Strong $\pi-\pi$ and van der Waals interactions facilitated the noncovalent encapsulation of nanoparticles by polydopamine, as confirmed by different characterization techniques such as SEM, TEM, TGA, and Raman spectroscopy. The prepared h-BN/BECy nanocomposites were investigated to determine the effect of volume fractions and functionalities of nanofillers on nanocomposite properties. The promising thermal stability of neat BECy was not compromised with the incorporation of h-BN nanoplatelets at any given loading levels. Because of their low CTE and superior storage modulus, the incorporated h-BN nanoparticles offered an improved dimensional stability and an outstanding reinforcement effect on the BECy resin, regardless of their functionality. Even though the dopamine-treated h-BN nanoperticles reduced the T_g of nanocomposite because of the lower chemical reactivity between the catechol moiety and the functional cyanate ester group, the pristine h-BN nanoparticles had nearly no detrimental effect on either cross-linking density or T_g. Incorporation of 15 vol % pristine nanoparticles caused the most pronouced improvement in thermal conductivity of h-BN/BECy nanocomposites. In addition, dielectric properties of nanocomposites could be tailored based on the functionalities of h-BN nanoparticles. In summary, the h-BN/BECy nanocomposites exhibited promising improvement in both thermomechanical and dynamic-mechanical properties, desirable enhancement in thermal conductivity, and controllable dielectric properties, indicating potential applications in microelectronic packaging and as structural capacitors for aerospace devices.

AUTHOR INFORMATION

Corresponding Author

*M. R. Kessler. E-mail: MichaelR.Kessler@wsu.edu.

Notes

The authors declare no competing financial interest.

ACKNOWLEDGMENTS

The authors acknowledge partial funding for this project by Honeywell Federal Manufacturing & Technologies, LLC and the Air Force Office of Scientific Research (Award No. FA9550-12-1-0108). The authors also acknolwedge Tacey Pepper (Genetics, Development & Cell Biology, Iowa State University) for her assitance with TEM measurement, and Landi Zhong (Materials Science and Engieering, Iowa State University) for the thermal conductivity measurement.

REFERENCES

(1) Luyt, A. S.; Molefi, J. A.; Krump, H. Thermal, Mechanical and Electrical Properties of Copper Powder Filled Low-Density Band Linear Low-Density Polyethylene Composites. *Polym. Degrad. Stab.* **2006**, *91*, 1629–1636.

(2) Huang, X. Y.; Iizuka, T.; Jiang, P. K.; Ohki, Y.; Tanaka, T. Role of Interface on the Thermal Conductivity of Highly Filled Dielectric Epoxy/Aln Composites. *J. Phys. Chem. C* **2012**, *116*, 13629–13639.

(3) Wu, H. Y.; Gu, A. J.; Liang, G. Z.; Yuan, L. Novel Permittivity Gradient Carbon Nanotubes/Cyanate Ester Composites with High Permittivity and Extremely Low Dielectric Loss. *J. Mater. Chem.* **2011**, *21*, 14838–14848.

(4) Han, C. F.; Gu, A. J.; Liang, G. Z.; Yuan, L. Carbon Nanotubes/Cyanate Ester Composites with Low Percolation Threshold, High Dielectric Constant and Outstanding Thermal Property. *Composites, Part A* **2010**, *41*, 1321–1328.

(5) Yuan, W.; Chan-Park, M. B. Covalent cum Noncovalent Functionalizations of Carbon Nanotubes for Effective Reinforcement of a Solution Cast Composite Film. *ACS Appl. Mater. Interfaces* **2012**, *4*, 2065–2073.

(6) Yuan, W.; Li, W. F.; Mu, Y. G.; Chan-Park, M. B. Effect of Side-Chain Structure of Rigid Polyimide Dispersant on Mechanical Properties of Single-Walled Carbon Nanotube/Cyanate Ester Composite. *ACS Appl. Mater. Interfaces* **2011**, *3*, 1702–1712.

(7) Yuan, W.; Feng, J. L.; Judeh, Z.; Dai, J.; Chan-Park, M. B. Use of Polyimide-Graft-Bisphenol a Diglyceryl Acrylate as a Reactive

DOI: 10.1021/acsami.5b00147
ACS Appl. Mater. Interfaces 2015, 7, 5915–5926

Noncovalent Dispersant of Single-Walled Carbon Nanotubes for Reinforcement of Cyanate Ester/Epoxy Composite. *Chem. Mater.* **2010**, *22*, 6542−6554.
(8) Liang, K. W.; Li, G. Z.; Toghiani, H.; Koo, J. H.; Pittman, C. U. Cyanate Ester/Polyhedral Oligomeric Silsesquioxane (POSS) Nanocomposites: Synthesis and Characterization. *Chem. Mater.* **2006**, *18*, 301−312.
(9) Shen, Y. P.; Gu, A. J.; Liang, G. Z.; Yuan, L. High Performance $CaCu_3Ti^4O_{12}$/Cyanate Ester Composites with Excellent Dielectric Properties and Thermal Resistance. *Composites, Part A* **2010**, *41*, 1668−1676.
(10) Chao, F.; Liang, G. Z.; Kong, W. F.; Zhang, X. Study of Dielectric Property on $BaTiO_3$/BADCy Composite. *Mater. Chem. Phys.* **2008**, *108*, 306−311.
(11) Lu, H. B.; Huang, W. M.; Leng, J. S. Functionally Graded and Self-Assembled Carbon Nanofiber and Boron Nitride in Nanopaper for Electrical Actuation of Shape Memory Nanocomposites. *Composites, Part B* **2014**, *62*, 1−4.
(12) Lu, H. B.; Yao, Y. T.; Huang, W. M.; Leng, J. S.; Hui, D. Significantly Improving Infrared Light-Induced Shape Recovery Behavior of Shape Memory Polymeric Nanocomposite via a Synergistic Effect of Carbon Nanotube and Boron Nitride. *Composites, Part B* **2014**, *62*, 256−261.
(13) Terao, T.; Bando, Y.; Mitome, M.; Zhi, C. Y.; Tang, C. C.; Golberg, D. Thermal Conductivity Improvement of Polymer Films by Catechin-Modified Boron Nitride Nanotubes. *J. Phys. Chem. C* **2009**, *113*, 13605−13609.
(14) Terao, T.; Zhi, C. Y.; Bando, Y.; Mitome, M.; Tang, C. C.; Golberg, D. Alignment of Boron Nitride Nanotubes in Polymeric Composite Films for Thermal Conductivity Improvement. *J. Phys. Chem. C* **2010**, *114*, 4340−4344.
(15) Zhi, C. Y.; Bando, Y.; Tang, C. C.; Huang, Q.; Golberg, D. Boron Nitride Nanotubes: Functionalization and Composites. *J. Mater. Chem.* **2008**, *18*, 3900−3908.
(16) Huang, X. Y.; Zhi, C. Y.; Jiang, P. K.; Golberg, D.; Bando, Y.; Tanaka, T. Polyhedral Oligosilsesquioxane-Modified Boron Nitride Nanotube based Epoxy Nanocomposites: An Ideal Dielectric Material with High Thermal Conductivity. *Adv. Funct. Mater.* **2013**, *23*, 1824−1831.
(17) Zhi, C. Y.; Bando, Y.; Tang, C. C.; Honda, S.; Sato, K.; Kuwahara, H.; Golberg, D. Characteristics of Boron Nitride Nanotube-Polyaniline Composites. *Angew. Chem., Int. Ed.* **2005**, *44*, 7929−7932.
(18) Song, W. L.; Wang, P.; Cao, L.; Anderson, A.; Meziani, M. J.; Farr, A. J.; Sun, Y. P. Polymer/Boron Nitride Nanocomposite Materials for Superior Thermal Transport Performance. *Angew. Chem., Int. Ed.* **2012**, *51*, 6498−6501.
(19) Cho, H. B.; Tu, N. C.; Fujihara, T.; Endo, S.; Suzuki, T.; Tanaka, S.; Jiang, W. H.; Suematsu, H.; Niihara, K.; Nakayama, T. Epoxy Resin-based Nanocomposite Films with Highly Oriented BN Nanosheets Prepared Using a Nanosecond-Pulse Electric Field. *Mater. Lett.* **2011**, *65*, 2426−2428.
(20) Cho, H. B.; Nakayama, T.; Tokoi, Y.; Endo, S.; Tanaka, S.; Suzuki, T.; Jiang, W. H.; Suematsu, H.; Niihara, K. Facile Preparation of a Polysiloxane-based Hybrid Composite with Highly-Oriented Boron Nitride Nanosheets and an Unmodified Surface. *Compos. Sci. Technol.* **2010**, *70*, 1681−1686.
(21) Yu, J. H.; Huang, X. Y.; Wu, C.; Wu, X. F.; Wang, G. L.; Jiang, P. K. Interfacial Modification of Boron Nitride Nanoplatelets for Epoxy Composites with Improved Thermal Properties. *Polymer* **2012**, *53*, 471−480.
(22) Zhou, W. Y.; Zuo, J.; Zhang, X. Q.; Zhou, A. N. Thermal, Electrical, and Mechanical Properties of Hexagonal Boron Nitride-Reinforced Epoxy Composites. *J. Compos. Mater.* **2014**, *48*, 2517−2526.
(23) Lin, Z. Y.; McNamara, A.; Liu, Y.; Moon, K. S.; Wong, C. P. Exfoliated Hexagonal Boron Nitride-based Polymer Nanocomposite with Enhanced Thermal Conductivity for Electronic Encapsulation. *Compos. Sci. Technol.* **2014**, *90*, 123−128.
(24) Hou, J.; Li, G. H.; Yang, N.; Qin, L. L.; Grami, M. E.; Zhang, Q. X.; Wang, N. Y.; Qu, X. W. Preparation and Characterization of Surface Modified Boron Nitride Epoxy Composites with Enhanced Thermal Conductivity. *RSC Adv.* **2014**, *4*, 44282−44290.
(25) Jin, W. Q.; Yuan, L.; Liang, G. Z.; Gu, A. J. Multifunctional Cyclotriphosphazene/Hexagonal Boron Nitride Hybrids and Their Flame Retarding Bismaleimide Resins with High Thermal Conductivity and Thermal Stability. *ACS Appl. Mater. Interfaces* **2014**, *6*, 14931−14944.
(26) Zeng, X. L.; Yu, S. H.; Sun, R. Thermal Behavior and Dielectric Property Analysis of Boron Nitride-filled Bismaleimide-Triazine Resin Composites. *J. Appl. Polym. Sci.* **2013**, *128*, 1353−1359.
(27) Huang, Y. C.; Lo, T. Y.; Chao, C. G.; Whang, W. T. Anti-corrosion Characteristics of Polyimide/H-Boron Nitride Composite Films with Different Polymer Configurations. *Surf. Coat. Technol.* **2014**, *260*, 113−117.
(28) Tanimoto, M.; Yamagata, T.; Miyata, K.; Ando, S. Anisotropic Thermal Diffusivity of Hexagonal Boron Nitride-filled Polyimide Films: Effects of Filler Particle Size, Aggregation, Orientation, and Polymer Chain Rigidity. *ACS Appl. Mater. Interfaces* **2013**, *5*, 4374−4382.
(29) Shoji, Y.; Higashihara, T.; Tokita, M.; Morikawa, J.; Watanabe, J.; Ueda, M. Thermal Diffusivity of Hexagonal Boron Nitride Composites Based on Cross-Linked Liquid Crystalline Polyimides. *ACS Appl. Mater. Interfaces* **2013**, *5*, 3417−3423.
(30) Xie, B. H.; Huang, X.; Zhang, G. J. High Thermal Conductive Polyvinyl Alcohol Composites with Hexagonal Boron Nitride Microplatelets as Fillers. *Compos. Sci. Technol.* **2013**, *85*, 98−103.
(31) Zhou, S. J.; Ma, C. Y.; Meng, Y. Y.; Su, H. F.; Zhu, Z.; Deng, S. L.; Xie, S. Y. Activation of Boron Nitride Nanotubes and Their Polymer Composites for Improving Mechanical Performance. *Nanotechnology* **2012**, *23*, 055708 (1−8).
(32) Velayudham, S.; Lee, C. H.; Xie, M.; Blair, D.; Bauman, N.; Yap, Y. K.; Green, S. A.; Liu, H. Y. Noncovalent Functionalization of Boron Nitride Nanotubes with Poly(p-phenylene-ethynylene)s and Polythiophene. *ACS Appl. Mater. Interfaces* **2010**, *2*, 104−110.
(33) Lee, H.; Dellatore, S. M.; Miller, W. M.; Messersmith, P. B. Mussel-Inspired Surface Chemistry for Multifunctional Coatings. *Science* **2007**, *318*, 426−430.
(34) Hong, S.; Na, Y. S.; Choi, S.; Song, I. T.; Kim, W. Y.; Lee, H. Non-covalent Self-Assembly and Covalent Polymerization Co-contribute to Polydopamine Formation. *Adv. Funct. Mater.* **2012**, *22*, 4711−4717.
(35) Fei, B.; Qian, B.; Yang, Z.; Wang, R.; Liu, W. C.; Mak, C. L.; Xin, J. H. Coating Carbon Nanotubes by Spontaneous Oxidative Polymerization of Dopamine. *Carbon* **2008**, *46*, 1795−1797.
(36) Song, Y.; Shen, Y.; Liu, H. Y.; Lin, Y. H.; Li, M.; Nan, C. W. Enhanced Dielectric and Ferroelectric Properties Induced by Dopamine-Modified $BaTiO_3$ Nanofibers in Flexible Poly(vinylidene fluoride-trifluoroethylene) Nanocomposites. *J. Mater. Chem.* **2012**, *22*, 8063−8068.
(37) Song, Y.; Shen, Y.; Liu, H. Y.; Lin, Y. H.; Li, M.; Nan, C. W. Improving the Dielectric Constants and Breakdown Strength of Polymer Composites: Effects of the Shape of the $BaTiO_3$ Nanoinclusions, Surface Modification and Polymer Matrix. *J. Mater. Chem.* **2012**, *22*, 16491−16498.
(38) Thakur, V. K.; Yan, J.; Lin, M. F.; Zhi, C. Y.; Golberg, D.; Bando, Y.; Sim, R.; Lee, P. S. Novel Polymer Nanocomposites from Bioinspired Green Aqueous Functionalization of BNNTs. *Polym. Chem.* **2012**, *3*, 962−969.
(39) Zhang, X. Y.; Ji, J. Z.; Zhang, X. Q.; Yang, B.; Liu, M. Y.; Liu, W. Y.; Tao, L.; Chen, Y. W.; Wei, Y. Mussel Inspired Modification of Carbon Nanotubes Using Raft Derived Stimuli-Responsive Polymers. *RSC Adv.* **2013**, *3*, 21817−21823.
(40) Gou, G.; Pan, B.; Shi, L. Noncovalent Functionalization of BN Nanotubes with Perylene Derivative Molecules: An Ab Initio Study. *ACS Nano* **2010**, *4*, 1313−1320.
(41) Lee, H.; Lee, Y.; Statz, A. R.; Rho, J.; Park, T. G.; Messersmith, P. B. Substrate-Independent Layer-by-Layer Assembly by Using

DOI: 10.1021/acsami.5b00147
ACS Appl. Mater. Interfaces 2015, 7, 5915−5926

Mussel-Adhesive-Inspired Polymers. *Adv. Mater.* **2008**, *20*, 1619−1620.
(42) Postma, A.; Yan, Y.; Wang, Y. J.; Zelikin, A. N.; Tjipto, E.; Caruso, F. Self-Polymerization of Dopamine as a Versatile and Robust Technique to Prepare Polymer Capsules. *Chem. Mater.* **2009**, *21*, 3042−3044.
(43) Wu, J.; Han, W. Q.; Walukiewicz, W.; Ager, J. W.; Shan, W.; Haller, E. E.; Zettl, A. Raman Spectroscopy and Time-Resolved Photoluminescence of BN and $B_xC_yN_z$ Nanotubes. *Nano Lett.* **2004**, *4*, 647−650.
(44) Gorbachev, R. V.; Riaz, I.; Nair, R. R.; Jalil, R.; Britnell, L.; Belle, B. D.; Hill, E. W.; Novoselov, K. S.; Watanabe, K.; Taniguchi, T.; Geim, A. K.; Blake, P. Hunting for Monolayer Boron Nitride: Optical and Raman Signatures. *Small* **2011**, *7*, 465−468.
(45) Ku, S. H.; Lee, J. S.; Park, C. B. Spatial Control of Cell Adhesion and Patterning through Mussel-Inspired Surface Modification by Polydopamine. *Langmuir* **2010**, *26*, 15104−15108.
(46) Shalev, T.; Gopin, A.; Bauer, M.; Stark, R. W.; Rahimipour, S. Non-leaching Antimicrobial Surfaces through Polydopamine Bio-inspired Coating of Quaternary Ammonium Salts or an Ultrashort Antimicrobial Lipopeptide. *J. Mater. Chem.* **2012**, *22*, 2026−2032.
(47) Lin, Z. Y.; Liu, Y.; Raghavan, S.; Moon, K. S.; Sitaraman, S. K.; Wong, C. P. Magnetic Alignment of Hexagonal Boron Nitride Platelets in Polymer Matrix: Toward High Performance Anisotropic Polymer Composites for Electronic Encapsulation. *ACS Appl. Mater. Interfaces* **2013**, *5*, 7633−7640.
(48) Badrinarayanan, P.; Kessler, M. R. Zirconium Tungstate/Cyanate Ester Nanocomposites with Tailored Thermal Expansivity. *Compos. Sci. Technol.* **2011**, *71*, 1385−1391.
(49) Goertzen, W. K.; Kessler, M. R. Thermal Expansion of Fumed Silica/Cyanate Ester Nanocomposites. *J. Appl. Polym. Sci.* **2008**, *109*, 647−653.
(50) Vennerberg, D.; Rueger, Z.; Kessler, M. R. Effect of Silane Structure on the Properties of Silanized Multiwalled Carbon Nanotube-Epoxy Nanocomposites. *Polymer* **2014**, *55*, 1854−1865.
(51) Sheng, X.; Akinc, M.; Kessler, M. R. Rheology and Dynamic Mechanical Analysis of Bisphenol E Cyanate Ester/Alumina Nanocomposites. *Polym. Eng. Sci.* **2010**, *50*, 302−311.
(52) Sun, W. X.; Sun, W. Z.; Kessler, M. R.; Bowler, N.; Dennis, K. W.; McCallum, R. W.; Li, Q.; Tan, X. L. Multifunctional Properties of Cyanate Ester Composites with SiO_2 Coated Fe_3O_4 Fillers. *ACS Appl. Mater. Interfaces* **2013**, *5*, 1636−1642.
(53) Putz, K. W.; Palmeri, M. J.; Cohn, R. B.; Andrews, R.; Brinson, L. C. Effect of Cross-Link Density on Interphase Creation in Polymer Nanocomposites. *Macromolecules* **2008**, *41*, 6752−6756.
(54) Huang, M. T.; Ishida, H. Surface Study of Hexagonal Boron Nitride Powder by Diffuse Reflectance Fourier Transform Infrared Spectroscopy. *Surf. Interface Anal.* **2005**, *37*, 621−627.
(55) Thakur, V. K.; Vennerberg, D.; Madbouly, S. A.; Kessler, M. R. Bio-inspired Green Surface Functionalization of PMMA for Multifunctional Capacitors. *RSC Adv.* **2014**, *4*, 6677−6684.
(56) Idicula, M.; Boudenne, A.; Umadevi, L.; Ibos, L.; Candau, Y.; Thomas, S. Thermophysical Properties of Natural Fibre Reinforced Polyester Composites. *Compos. Sci. Technol.* **2006**, *66*, 2719−2725.
(57) Yung, K. C.; Zhu, B. L.; Wu, J.; Yue, T. M.; Xie, C. S. Effect of Aln Content on the Performance of Brominated Epoxy Resin for Printed Circuit Board Substrate. *J. Polym. Sci., Part B: Polym. Phys.* **2007**, *45*, 1662−1674.
(58) Lewis, T. B.; Nielsen, L. E. Dynamic Mechanical Properties of Particulate-filled Composites. *J. Appl. Polym. Sci.* **1970**, *14*, 1449−1471.
(59) Progelhof, R. C.; Throne, J. L.; Ruetsch, R. R. Methods for Predicting the Thermal Conductivity of Composite Systems: A Review. *Polym. Eng. Sci.* **1976**, *16*, 615−625.
(60) Pal, R. On the Lewis-Nielsen Model for Thermal/Electrical Conductivity of Composites. *Composites, Part A* **2008**, *39*, 718−726.
(61) Thakur, V. K.; Lin, M. F.; Tan, E. J.; Lee, P. S. Green Aqueous Modification of Fluoropolymers for Energy Storage Applications. *J. Mater. Chem.* **2012**, *22*, 5951−5959.

DOI: 10.1021/acsami.5b00147
ACS Appl. Mater. Interfaces 2015, 7, 5915−5926